Histamine interferes with the early visual processing in mice

Authors: Matteo Tripodi[1], Hiroki Asari*[1]

Affiliations:

1. Epigenetics and Neurobiology Unit, EMBL Rome, European Molecular Biology Laboratory, Monterotondo, 00015, Italy

***Corresponding author:** Hiroki Asari, E-mail: asari@embl.it

Author contributions: M.T. and H.A. designed the study; M.T. performed experiments; M.T. and H.A. analyzed the results; and M.T. and H.A. wrote the manuscript.

Competing interests: The authors declare no competing financial interests.

Key words: retinal ganglion cells; lateral geniculate nucleus; histaminergic modulation; tuberomammillary nucleus.

Acronyms: AAV, adeno-associated virus; ANOVA, analysis of variance; DLP, digital light processing; DRN, dorsal raphe nucleus; HDC, histidine decarboxylase; GABA, γ-aminobutyric acid; IQR, interquartile range; IR, infrared; LED, light emitting diode; LGN, lateral geniculate nucleus; OT, optic tract; PFA, paraformaldehyde; PSAM/PSEM, pharmacologically selective actuator/effector module; RF, receptive field; RGC, retinal ganglion cell; STA, spike-triggered average; tSNE, t-distributed Stochastic Neighbor Embedding; UV, ultraviolet.

Abstract

Sensory processing is dynamically modulated by an animal's behavior and internal states. Growing evidence suggests that such modulation starts from early stages, even at the retina, but the underlying mechanisms remain elusive. Combining pharmacological and chemogenetic tools with single-unit extracellular recordings in awake head-fixed mice, here we identified that the visual responses of retinal ganglion cells and the lateral geniculate nucleus were both made weaker and slower by histaminergic projections from the tuberomammillary nucleus of the posterior hypothalamus. The observed changes in the visual responses were, however, not directly linked with histaminergic modulation of pupil dynamics or locomotion behavior. Instead, our computational modelling analysis suggests neuronal circuit effects, such as gain modulation via the H1 receptors in the retina. As nocturnal animals, facilitation of visual processing at low histamine level will be ethologically beneficial for mice to respond faster to visual threats when animals are less active during daytime.

Introduction

In the mammalian brain, histaminergic neurons are exclusively located in the tuberomammillary nucleus (TMN) and surrounding areas of the posterior hypothalamus (Haas and Panula, 2003). They express histidine decarboxylase (HDC) and innervate most brain regions, including the retina (Lin et al., 2023). These neurons remain silent during sleep, but increase their firing during wakefulness and reach their maximal activity at the state of high vigilance, much as other monoaminergic systems do, such as the serotonergic neurons in the dorsal raphe nucleus (DRN) of the brain stem (Lin et al., 2023; Takahashi et al., 2006; Thakker, 2011). Brain histamine exerts its effects via three types of receptors: the H1 and H2 receptors mediate excitation of postsynaptic cells, while the H3 receptors serve as an auto-receptor to presynaptically inhibit histamine release (Haas and Panula, 2003). The histaminergic system has been implicated in regulating an animal’s state and a broad range of behavior, including the sleep-wake cycle (John et al., 2004; Mochizuki et al., 1992), arousal (Parmentier et al.,

2002; Scammell et al., 2018), suppression of food intake (Khouma et al., 2023; Valdés et al., 2010; Wang et al., 2015) and learning (Kamei et al., 1993; Klapdor et al., 1994; Orsetti et al., 2001; Rubio et al., 2002). Histaminergic neurons, however, corelease γ-aminobutyric acid (GABA) and interact with other neuromodulator systems, such as the cholinergic and serotonergic systems (Brown et al., 2002; Khateb et al., 1995; Lin et al., 2023). This makes it difficult to dissect the effects of histamine alone on neural circuit functions. In particular, histaminergic modulation of sensory processing remains largely elusive.

The retina performs the first stage of visual processing, and conveys visual information to the brain via spike trains of retinal ganglion cells (RGCs). Growing evidence supports that the activity of RGCs is correlated with various behavioral measures, such as locomotion and pupil size (Schröder et al., 2020; Liang et al., 2020; Reggiani et al., 2023; Boissonnet et al., 2023), pointing to a more dynamic role of the retina than is often assumed as a deterministic processor. The vertebrate retina is part of the central nervous system equipped with both intrinsic and extrinsic neuromodulation mechanisms, much as other brain regions do (Lee & Dan, 2012; McCormick et al., 2020). For instance, dopamine is synthesized and released by a group of retinal amacrine cells under the control of circadian rhythm, and contributes to adjusting the retinal circuitry for rod/cone vision by modulating gap-junction couplings (Bloomfield & Völgyi, 2009). Such retinal intrinsic mechanisms of neuromodulation are, however, much slower than needed to modulate retinal function to follow rapid behavioral changes. To this end, the retina seems to exploit the centrifugal system to receive inputs from a variety of brain regions in a species-specific manner (Repérant et al., 2007). For example, histaminergic and serotonergic projections from the tuberomammillary nucleus (TMN) of the hypothalamus and dorsal raphe nucleus in the brain stem, respectively, have been identified in the mammalian retina (Gastinger et al., 1999; Greferath et al., 2009; Labandeira-Garcia et al., 1990; Warwick et al., 2024). However, compared to the isthmo-optic pathway in birds (Wilson and Lindstrom, 2011) or the olfacto-retinal circuit in fish (Esposti, et al., 2013), little is known about the function of the mammalian centrifugal system.

Combining in vivo single-unit extracellular recordings from either the lateral geniculate nucleus (LGN) or the optic tract (OT) with pharmacological and chemogenetic tools, here we explored how histamine affects the early visual processing in awake head-fixed mice. During the recording sessions, we simultaneously monitored the subject animal's behavior, such as pupil dynamics and locomotion, to better correlate the effects of histamine on the visual response properties with those on the behavioral measures. We also took a computational approach to clarify the net effect of histamine on the visual responses from functional viewpoints. Because visual processing in the brain fully relies on the signals from the retina, understanding of the retinal operation in vivo is indispensable to better characterize and model how the visual system works.

Results

Histamine led to weaker and slower visual responses in the mouse lateral geniculate nucleus

To investigate how histamine influences the mouse visual system, we first performed in vivo single-unit extracellular recordings from the lateral geniculate nucleus (LGN) in awake head-fixed mice, and compared the visual response properties of the recorded cells before and after perturbing the central histaminergic system (Figure 1A; see Methods for details). Stimulus ensemble statistical techniques ("reverse correlation"; Chichilnisky, 2001) were employed to systematically characterize the visual response properties of the recorded cells in the framework of a linear-nonlinear cascade model (Boissonnet et al., 2023). In particular, using full-field white-noise stimuli, we analyzed histaminergic effects on 1) the linear temporal filter, estimated by the spike-triggered average (STA) stimulus, i.e., the mean stimulus that triggered spiking responses; and 2) the static nonlinear gain function, i.e., an instantaneous mapping of the STA output to the neural responses (Figure 1B). We also functionally mapped the cells' receptive field (RF) by calculating the linear spatial filter from the responses to random

79 “checkerboard” stimuli, where each square randomly and independently flickered over time.
80 To manipulate the histaminergic system, we used two different approaches (Supplementary
81 Figure 1). The first is the chemogenetic activation of the central histaminergic system (Magnus
82 et al., 2011). We injected cre-dependent adeno-associated viruses (AAVs) carrying
83 pharmacologically selective actuator module (PSAM)-5HT3HC channels into the
84 tuberomammillary nucleus (TMN) of the posterior hypothalamus in histidine decarboxylase
85 (HDC)-cre transgenic mice, and then achieved selective activation of the target neurons by
86 systemic administration of the pharmacologically selective effector molecule (PSEM). The
87 second approach is the use of pharmacological tools in wild-type mice (Thakkar, 2011).
88 Specifically, we used chlorphenamine (5 mg/kg), an antagonist of a postsynaptic histamine
89 receptor H1; and ciproxifan (12 mg/kg), an antagonist of the H3 auto-receptor that
90 presynaptically inhibits histamine release. These drugs effectively down- and up-regulate the
91 action of histamine in the nervous system, respectively. Thus, resulting changes in visual
92 processing, if any, were expected to be in opposite directions.

93 Upon chemogenetically activating HDC+ neurons in TMN, we found that LGN neurons
94 generally showed weaker and slower visual responses (Figure 1C,F). The mean firing rate
95 during the visual stimulation significantly reduced (median, -5.0 Hz; interquartile range (IQR),
96 9.9 Hz; p(U-test)<0.001, N=58 from 3 animals); and the response gain also significantly
97 decreased (median, -41%; IQR, 54%; p(U-test)<0.001) that was computed as the ratio of the
98 estimated static nonlinearity functions before and after PSEM injection. The temporal filter
99 became elongated regardless of their functional cell types (Supplementary Figure 2), leading
100 to significantly longer peak latencies (median, +32 ms; IQR, 27 ms; p(U-test)<0.001) and lower
101 peak frequencies (median, -16%; IQR, 5 %; p(U-test)=0.01).

102 Consistent results were obtained when histamine release was pharmacologically up-
103 regulated. Specifically, after the application of ciproxifan (H3 blocker; Figure 1D,G), we found
104 significantly reduced mean firing rates (median, -3.7 Hz; IQR, 5.0 Hz; p(U-test)<0.001, N=48
105 from 2 animals) and response gain (median, -30%; IQR, 52%; p(U-test)=0.003), significantly

longer peak latency (median, +17 ms; IQR, 13 ms; p(U-test)<0.001) and lower peak frequency (median, -9%; IQR, 14 %; p(U-test)<0.001) of the linear temporal filters. These effects of the pharmacological treatment were less prominent than those of the chemogenetic manipulation (Figure 1I-L), except for the changes in the receptive field size where the reduction reached the statistically significant level with ciproxifan (median, -26%; IQR, 38 %; p(U-test)=0.004, N=28 from 2 animals) but not with PSAM/PSEM procedure (median, -11%; IQR, 32 %; p(U-test)=0.11, N=19 from 2 animals; Supplementary Figure 3A-F).

In contrast, chlorphenamine (H1 antagonist; Figure 1E,H) led to marginal changes in the visual response properties of LGN neurons in the opposite direction. We observed a tendency towards an increased mean evoked firing rate (median, +1.0 Hz; IQR, 7.2 Hz; p(U-test)=0.09, N=116 from 3 animals) and response gain (median, +13%; IQR, 87%; p(U-test)=0.3), and facilitated response kinetics with significantly higher peak frequency of the linear temporal filter (median, +4%; IQR, 15%; p(U-test)=0.03) but no significant changes in its peak latency (median, 0 ms; IQR, 5 ms; p(U-test)=0.7) or the receptive field size ((median, +5%; IQR, 34 %; p(U-test)=0.08, N=38 from 3 animals; Figure 1I-L and Supplementary Figure 3A-F). Taken together, these results indicate that the more the histamine, the lower the response gain and the faster the response kinetics in the mouse LGN.

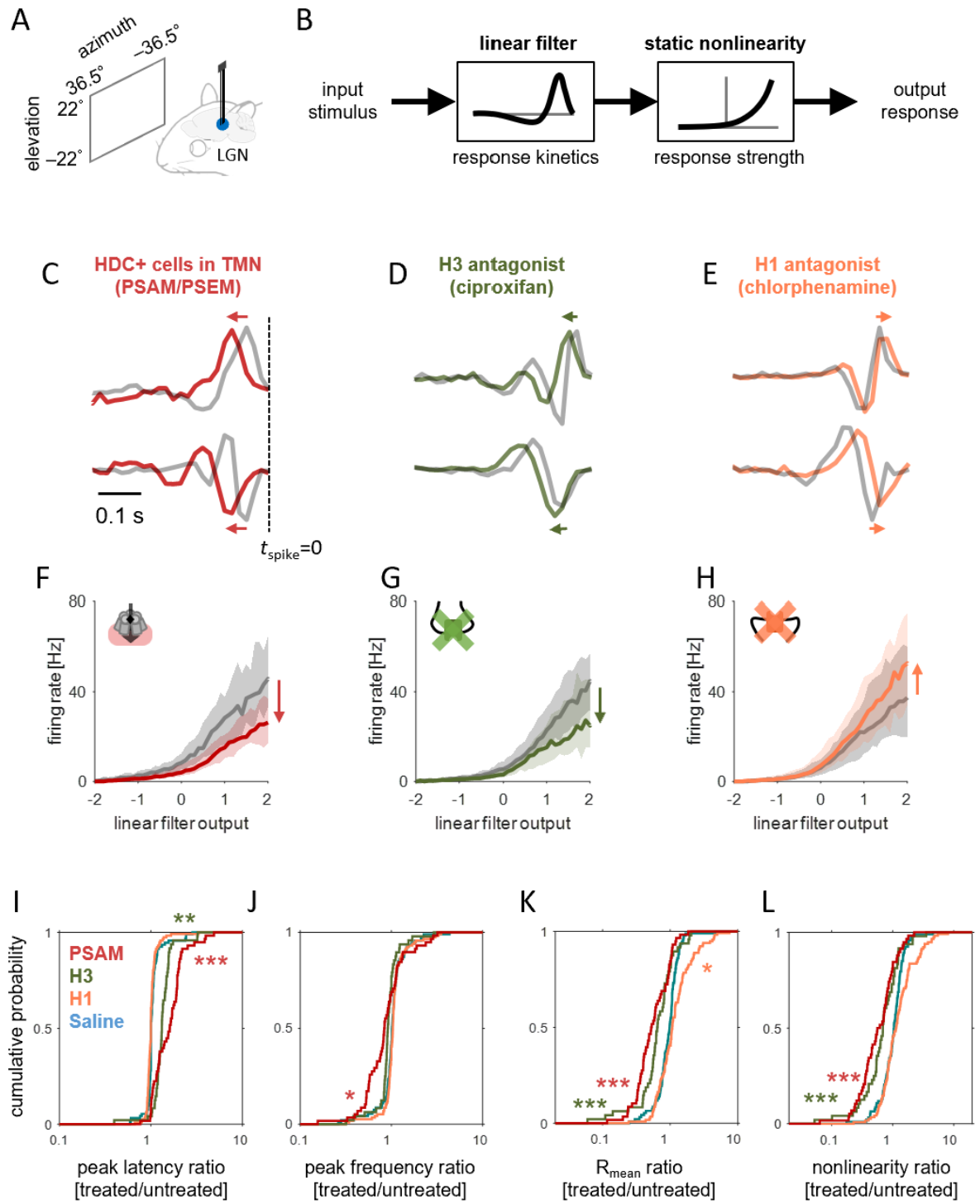

Figure 1: histamine made the visual responses of LGN weaker and slower in awake head-fixed mice. *A,B*: schematic diagram of LGN recordings (A) and linear-nonlinear cascade model (B). Reverse-correlation was used to estimate the linear filter and static nonlinearity that represent response kinetics and strength, respectively. *C*: linear filters of two representative LGN cells before (gray) and after chemogenetic activation of HDC+ cells in TMN (red). *D,E*: representative LGN linear filters before (gray) and after pharmacological treatment (D, 12 mg/kg ciproxifan, green; E, 5 mg/kg chlorphenamine, orange). *F-H*: static nonlinearities averaged across LGN population before and after treatment in corresponding

colors (F, chemogenetics, N=58 from 3 animals; G, ciproxifan, N=48 from 2 animals; H, chlorphenamine, N=116 from 3 animals). *I-L*: cumulative distributions of response feature ratio before and after each treatment (in corresponding color): peak latency (I) and frequency (J) of the linear temporal filters, mean evoked firing rate during stimulation (K), and static nonlinearity (i.e., response gain; L). One-way analysis of variance (ANOVA) with Tukey-Kramer correction was used to compute the p-value against saline control (blue, N=93 from 3 animals): *, p<0.05; **, p<0.01; ***, p<0.001.

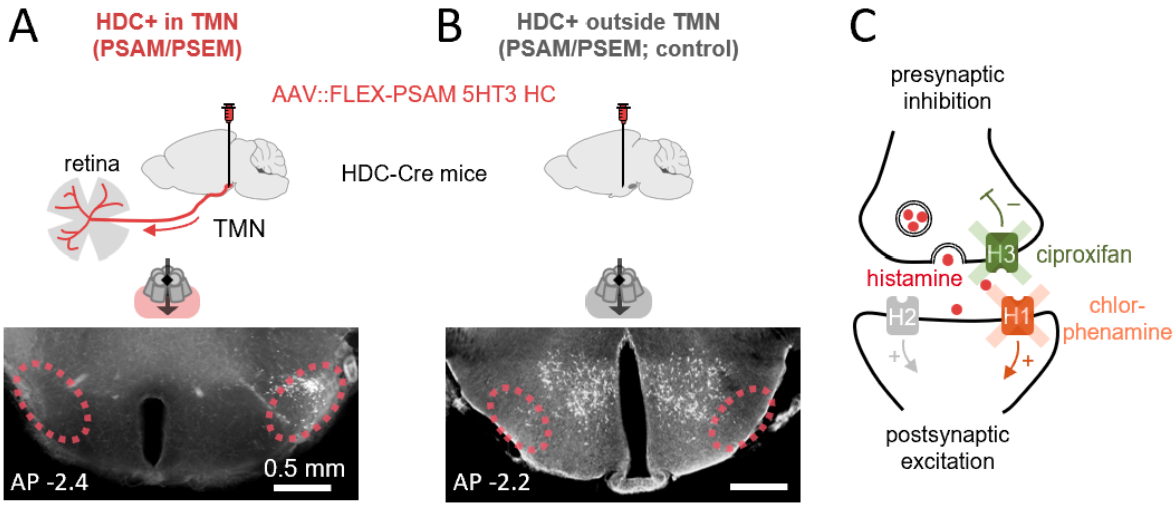

Supplementary Figure 1: Pharmacological and chemogenetic approaches to manipulate the central histaminergic system in the mouse brain. *A,B*: Viral delivery of PSAM 5HT3HC channel to HDC+ cells in the TMN (marked with dotted lines) of the posterior hypothalamus (A) or those in the anterior hypothalamus (B; control). *C*: schematic diagram of histamine receptor localizations and their cellular function. Chlorphenamine blocks the postsynaptic receptor H1 (orange) that mediates the action of histamine postsynaptically, while ciproxifan blocks the auto-receptor H3 (green) that inhibits presynaptic histamine release.

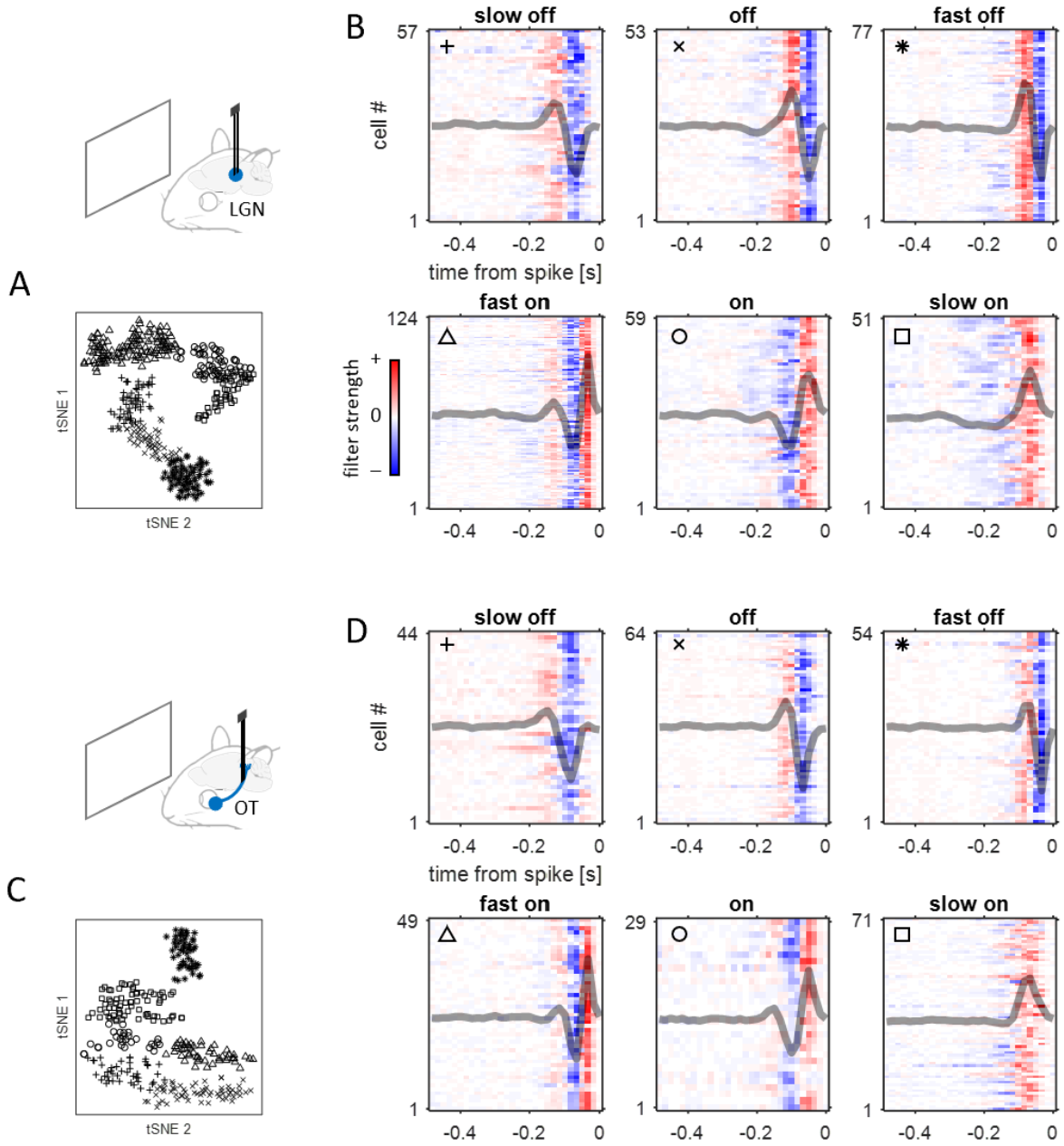

Supplementary Figure 2: functional classification of LGN/RGC visual response types. *A*: t-SNE embedding of the STAs of LGN cells. Different markers are used for distinct response categories (shown in B). *B*: Each panel represents one of the six response categories: slow off, off, fast off, fast on, on, and slow on. In each panel, each row represents a cell's STA (color-coded with red and blue indicating positive and negative filter values, respectively); and the overlaid gray line shows the average STAs in each response type. *C,D*: corresponding data for RGCs obtained by in vivo optic tract (OT) recordings methods.

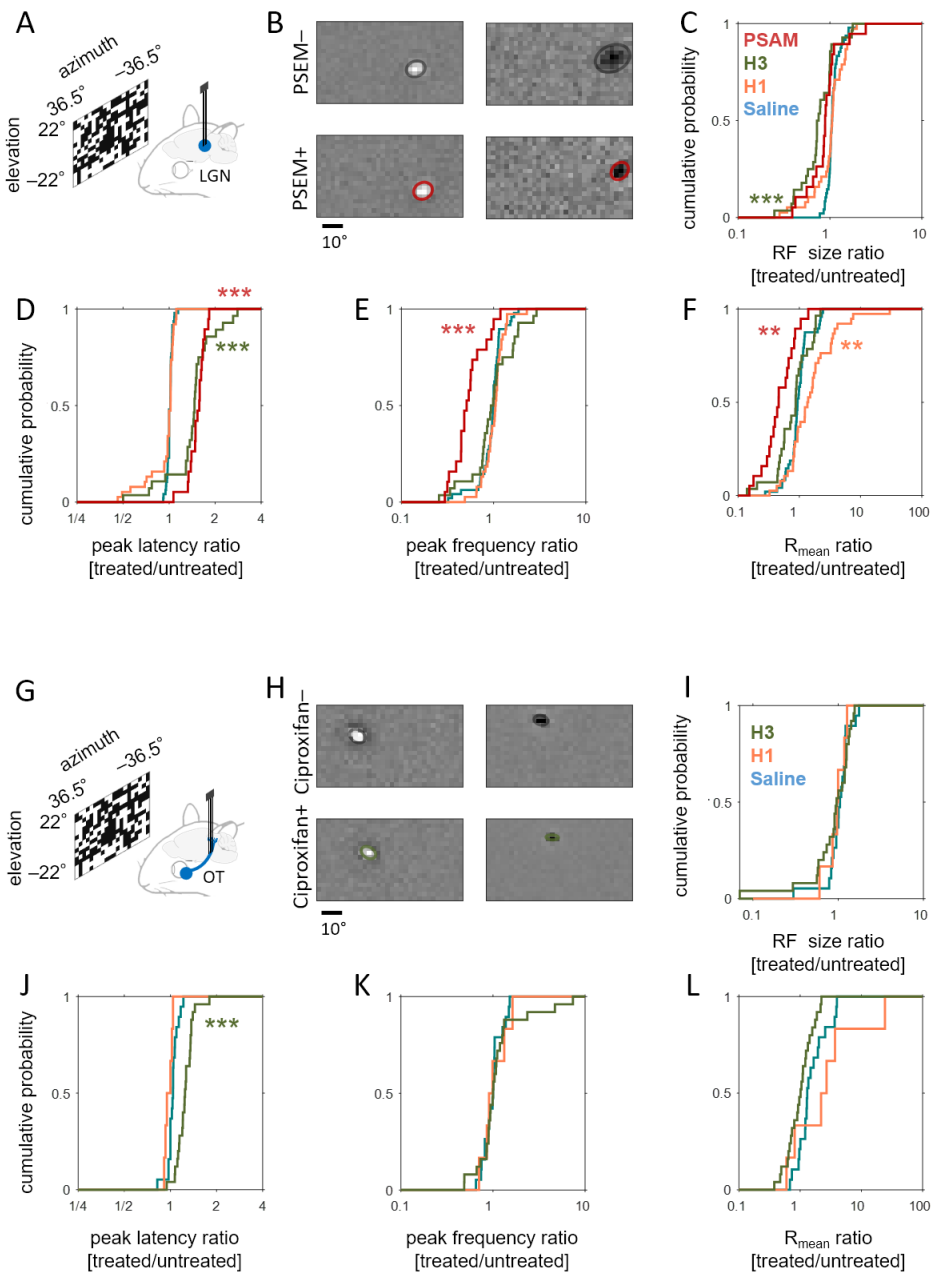

Supplementary Figure 3: Histamine made the LGN RFs smaller but not RGC RFs. *A*: schematic diagram of LGN recordings with white-noise "checkerboard" stimuli. *B*: estimated spatial filter (receptive field) of two example LGN cells before (top) and after (bottom) chemogenetic activation of HDC+ cells in TMN. Note a decrease of the RF size of this OFF LGN cell (right), while no change was observed for this ON cell (left). *C-F*: cumulative distribution of the RF size ratio of LGN cells before and after treatment (C; orange, chlorphenamine, N=38 from 3 animals; green, ciproxifan, N=28 from 2 animals; red, PSAM/PSEM for HDC+ cells in TMN, N=19 cells from 2 animals) and corresponding figure panels for the peak latency (D) and frequency (E) of the RF center dynamics as well as for the mean firing rate (F). One-way ANOVA with Tukey-Kramer correction against saline control (N=48 from 3 animals): *, p<0.05; **, p<0.01; ***, p<0.001. *G-L*: corresponding figure panels for RGCs: chlorphenamine (H1 antagonist), N=6 from 3 animals; ciproxifan (H3 antagonist), N=25 from 4 animals; saline, N=18 from 3 animals.

Histaminergic modulation starts from the mouse retina

Histaminergic neurons are localized solely in the hypothalamus, most densely in TMN, and project their axons widely across the brain (Lin et al., 2023), including the mouse retina (Gastinger et al., 1999; Repérant et al., 2007; Warwick et al., 2024). To test if the observed histaminergic modulation of the visual processing in LGN originates in the retina, we next performed in vivo optic tract (OT) recordings to monitor the retinal output responses in awake head-fixed mice (Boissonnet et al., 2023) before and after manipulating the central histaminergic system (Figure 2).

Consistent with the results in LGN, chemogenetic activation of HDC+ neurons in TMN led to reduced firing (median, -13.0 Hz; interquartile range (IQR), 25.5 Hz; p(U-test)=0.11, N=10 from 2 animals) with lower response gain (median, -51%; IQR, 50 %; p(U-test)=0.04), and slower response kinetics with elongated linear temporal filters (peak latency change, median, 46 ms; IQR, 22 ms; p(U-test)=0.008; peak frequency change, median, -36%; IQR, 22%, p(U-test)=0.04) for retinal ganglion cells (RGCs) as well (Figure 2A,D). In contrast, no change in these response parameters was observed when targeting HDC+ populations in the anterior hypothalamus outside TMN for the PSAM/PSEM activation (firing change, median, -0.7 Hz, IQR, 16 Hz, p(U-test)=1; gain change, median, 0.5%, IQR, 79%, p(U-test)=1; latency change, median +2 Hz, IQR, 11 Hz, p(U-test)=0.8; frequency change, median -2.9%, IQR, 11%, p(U-test)=0.12; N=23 from 3 animals). This supports that the histaminergic modulation of the early visual system is mediated by the centrifugal projections from TMN (Figure 2G-J and Supplementary Figure 1).

The effects of the pharmacological treatments were overall similar between LGN and RGCs, though certain differences existed. First, pharmacologically blocking the H3 receptors with ciproxifan led to slower response kinetics in both LGN and RGCs (N=40 from 4 animals; latency change, median, 8 ms; IQR, 14 ms; p(Utest)<0.001; frequency change, median, -7%; IQR, 19%; p(U-test)=0.04), but the firing rates (median -0.3 Hz; IQR, 14.2 Hz; p(U-text)=0.8) and the response gain (median, -1.3%; IQR, 68%, p(Utest)=0.8) remained largely unaffected

in RGCs (Figure 2B,E). Second, while chlorphenamine (H1 antagonist) drove faster kinetics with marginally higher firing in both LGN and RGCs, the effects on the temporal filters were primarily on the peak latencies in RGCs, but on the peak frequencies in LGN (Figure 2C,F; latency change, median, -5 ms; IQR, 10 ms; p(U-test)=0.004; frequency change, median, +4 Hz; IQR, 19 Hz; p(U-test)=0.7; firing change, median, +2.1 Hz, IQR, 10.4 Hz; p(U-test)=0.14; gain change, median, 5%, IQR, 88&, p(U-test)=0.2; N=34 RGCs from 3 animals). Finally, RGC receptive fields did not show significant changes in size (Supplementary Figure 3G-L). Taken together, our electrophysiology data indicate that 1) the mouse early visual processing is subject to histaminergic modulation controlled by TMN, starting from the retina; and 2) histamine generally suppresses the firing and slows the response kinetics, where response latency and frequency tuning are likely modulated by different mechanisms.

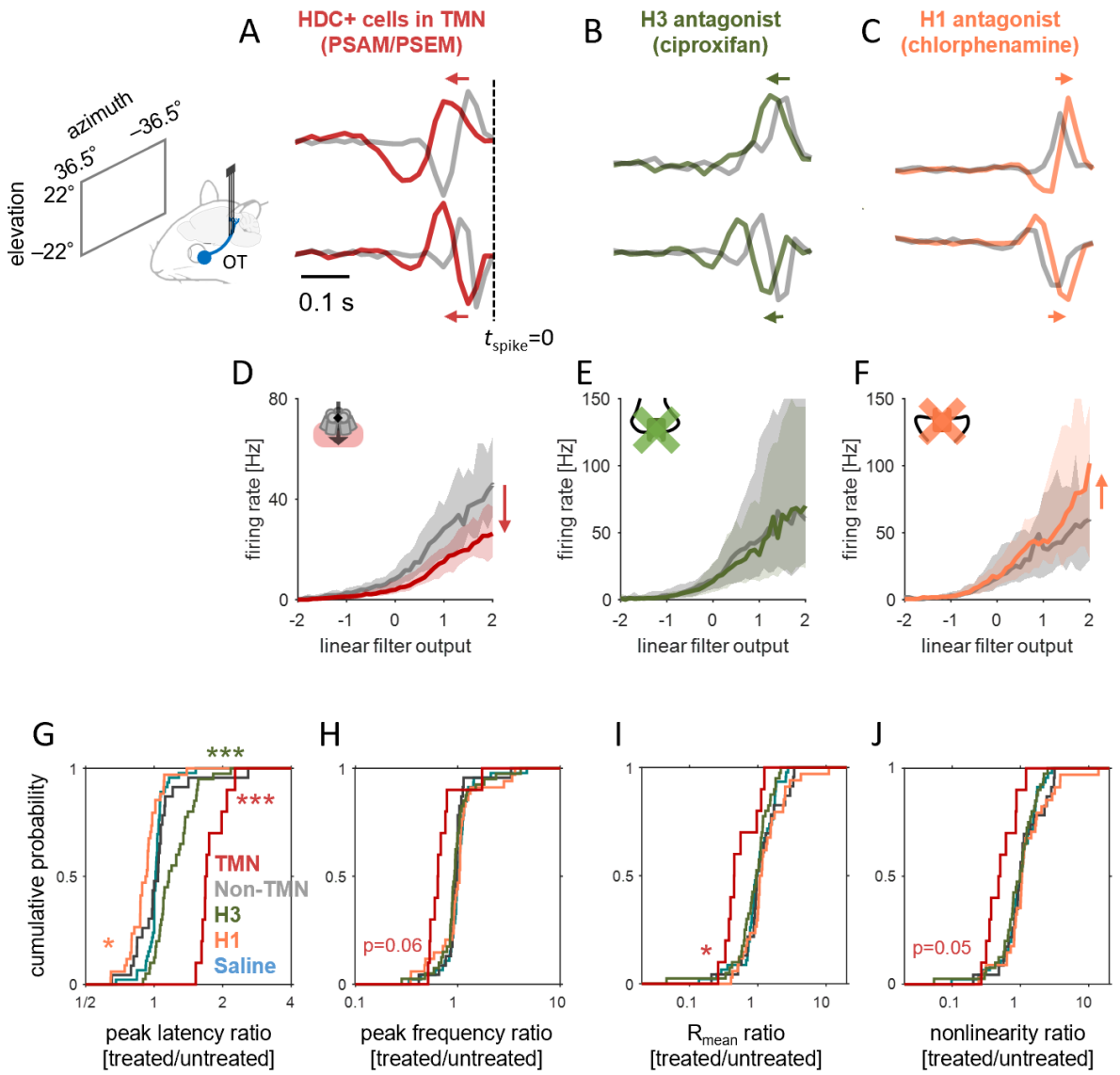

Figure 2: histamine primarily modulated the visual response kinetics of RGCs. *A-C*: linear filters of two representative RGCs before (gray) and after chemogenetic (A) or pharmacological treatment (B, ciproxifan, green; C, chlorphenamine, orange). Schematic diagram of in vivo optic tract (OT) recordings is displayed on the left. *D-F*: static nonlinearities averaged across RGC population before and after treatment in corresponding colors (D, chemogenetics, N=10 from 2 animals; E, ciproxifan, N=40 from 4 animals; F, chlorphenamine, N=34 from 3 animals). *G-J*: cumulative distributions of the response feature ratio before and after each treatment (in corresponding colors): peak latency (G) and frequency (H) of the linear temporal filters, mean evoked firing rate during stimulation (I), and static nonlinearity gain function (J). One-way ANOVA with Tukey-Kramer correction (chemogenetics against non-TMN targets, N=23 from 3 animals, dark gray; pharmacology against saline control, N=46 from 4 animals, blue): *, p<0.05; **, p<0.01; ***, p<0.001.

Pupil dynamics and locomotion are irrelevant to histaminergic modulation of the early visual processing

Histamine is a potent neuromodulator implicated in various brain functions and behaviors, such as sleep-wake cycles and arousal (Haas and Panula, 2003; Thakkar, 2011). We then cannot deny a possibility that the observed histaminergic effects on the visual response properties in the mouse early visual system are rather by-products due to the consequences of behavioral modulation. For example, the larger the pupil size, the more photons the retina receives, hence the stronger the responses (Biossonnet et al., 2023). To address this issue, we examined the relationship between the histaminergic effects on the RGC/LGN visual responses and simultaneously monitored behavioral measures (Figure 3).

We first analyzed the histaminergic modulation of pupil dynamics (Figure 3A), and found pupil dilation in all 6 mice after chlorphenamine (H1 antagonist) application, whereas pupil constriction in 7 out of 8 animals when histamine release was enhanced by systemic injection of ciproxifan (H3 antagonist). Chemogenetic activation of the central histaminergic system, however, led to pupil dilation in most animals (4 out of 5 mice). Thus, the polarity of the changes in pupil size was not consistent with that of RGC/LGN visual responses. This suggests that the histaminergic modulation of the pupil size cannot explain that of the early visual processing.

We next examined how histamine affects locomotion behavior of the head-fixed animals on the treadmill during recordings (Figure 3B,C). These mice often stayed still and moved fast ("running" at >2 cm/s) only about 20% of the time on average. In general, regardless of the methods, histaminergic perturbations did not strongly affect the amount of time spent without running in most mice (Figure 3B). If they did, however, we found that the chemogenetic activation of HDC+ neurons in TMN resulted in a substantial increase of no-running periods (2 out of 6 mice), whereas both chlorphenamine and ciproxifan led to a substantial decrease (2 out of 6 and 1 out of 7 mice, respectively). Furthermore, the mean

running speed during the recordings decreased upon the chemogenetic activation, whereas it varied in both directions after the pharmacological treatments (Figure 3C). Thus, changes in locomotion behavior driven by histamine were no in agreement with the histaminergic effects on the RGC/LGN visual responses (Figures 1 and 2).

Taken together, neither pupil dynamics nor locomotion behavior was causally linked with the histaminergic modulation of the mouse early visual system. Therefore, we conclude that the central histaminergic system indeed modulates the mouse vision, effectively making the responses slower and weaker.

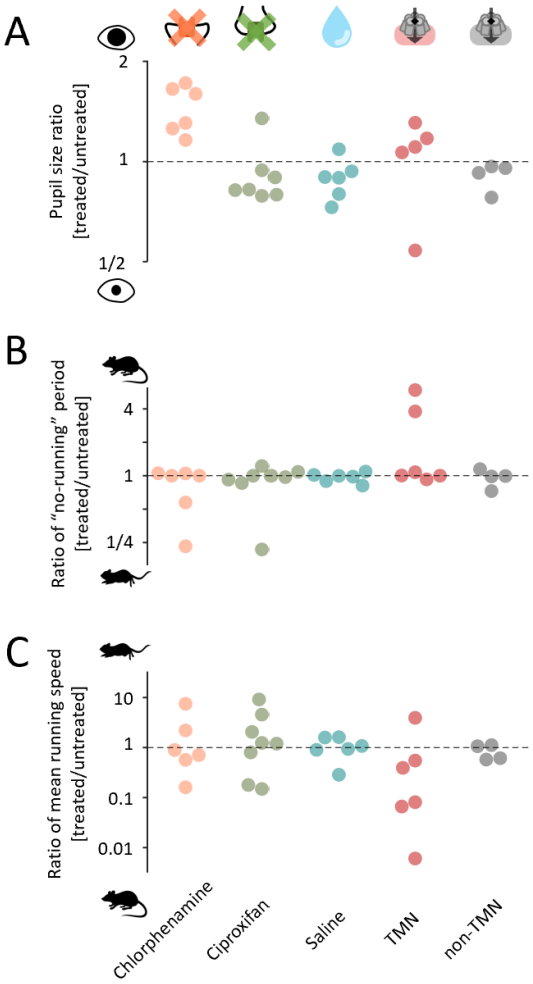

Figure 3: histaminergic modulation of pupil dynamics and locomotion behavior was not causally linked with that of RGC/LGN visual responses. *A*: the ratio of the average pupil size before and after treatment (in corresponding colors). *B*: the ratio of the "no-running" periods (threshold, 2 cm/s) before and after treatment. *C*: the ratio of the average locomotion speed during recording sessions before and after treatment.

Response gain modulation is more strongly correlated with peak latency modulation than with peak frequency modulation

What are the mechanisms underlying the histaminergic modulation of visual processing? To address this question, we next took a computational approach to examine the relationship between different aspects of the visual response properties that we identified were affected by histamine (Figure 4). In particular, we simulated the activity of an integrate-and-fire neuron with Poisson spiking and refractoriness in response to white-noise input stimuli (Figure 4A), and processed the output spike trains in the framework the linear-nonlinear cascade model to characterize the simulated response properties in the same way as the experimental data (Figure 1A). Here we varied two model parameters, gain and resting baseline, to examine the effects of their changes on the following four aspects of the simulated responses: spike counts, the peak latency and frequency of the estimated linear temporal filter, and the slope of the estimated static nonlinearity expressed as half-wave rectification. The rest model parameters were fixed in all simulations, including the underlying linear filter given by a cosine function with logarithmic scale in time, and the refractory period filter given by an exponential function. The spike threshold was drawn from a random uniform distribution ranging from 0 to 1 for each time point to approximate the Poisson spiking properties.

When the model neuron had a higher gain or higher resting baseline, subthreshold signal reached the spike threshold faster and more frequently; hence, total spike counts became higher (Figure 4B) and the peak latency of the estimated linear temporal filter appeared shorter (Figure 4C). In contrast, the apparent peak frequency of the simulated responses was dependent more strongly on the resting baseline than on the gain (Figure 4D). These changes in the estimated linear temporal filter properties were consistent with the experimental observation, where the magnitude of the response gain modulation by histamine perturbation was significantly correlated with that of the peak latency modulation (Figure 4F,H),

286 but much less with that of the peak frequency modulation (Figure 4G,I). This agreement
287 between the observed and simulated data indicates that, despite the simplicity, our model
288 captures aspects of neuronal response modulation to a first approximation.

289 The model analysis supports that the histaminergic effects on RGCs should involve at
290 least gain and baseline modulations. First, the H1 receptors likely mediate the gain modulation
291 in RGCs, given that chlorphenamine (H1 antagonist) led to changes in the peak latency but
292 not the peak frequency, along with changes in the estimated static nonlinearity largely by
293 scaling (Figure 2). Second, the peak frequencies were modulated as well as the peak latencies
294 of RGCs upon chemogenetic activation of HDC+ neurons in TMN, accompanied by a shift of
295 the estimated static nonlinearity. This implies changes in the baseline resting potential of the
296 cells. Blocking the H3 receptors, however, led to changes in the RGC response kinetics
297 without much affecting the mean firing rates. Furthermore, the net effects of histamine
298 perturbations on LGN responses were more diverse (Figure 1) and not fully explainable by the
299 simple model (Figure 4). Thus, we expect that mechanisms besides gain and baseline
300 modulations are also involved, such as neural circuit effects through retinal amacrine cells for
301 example (Horio et al., 2018).

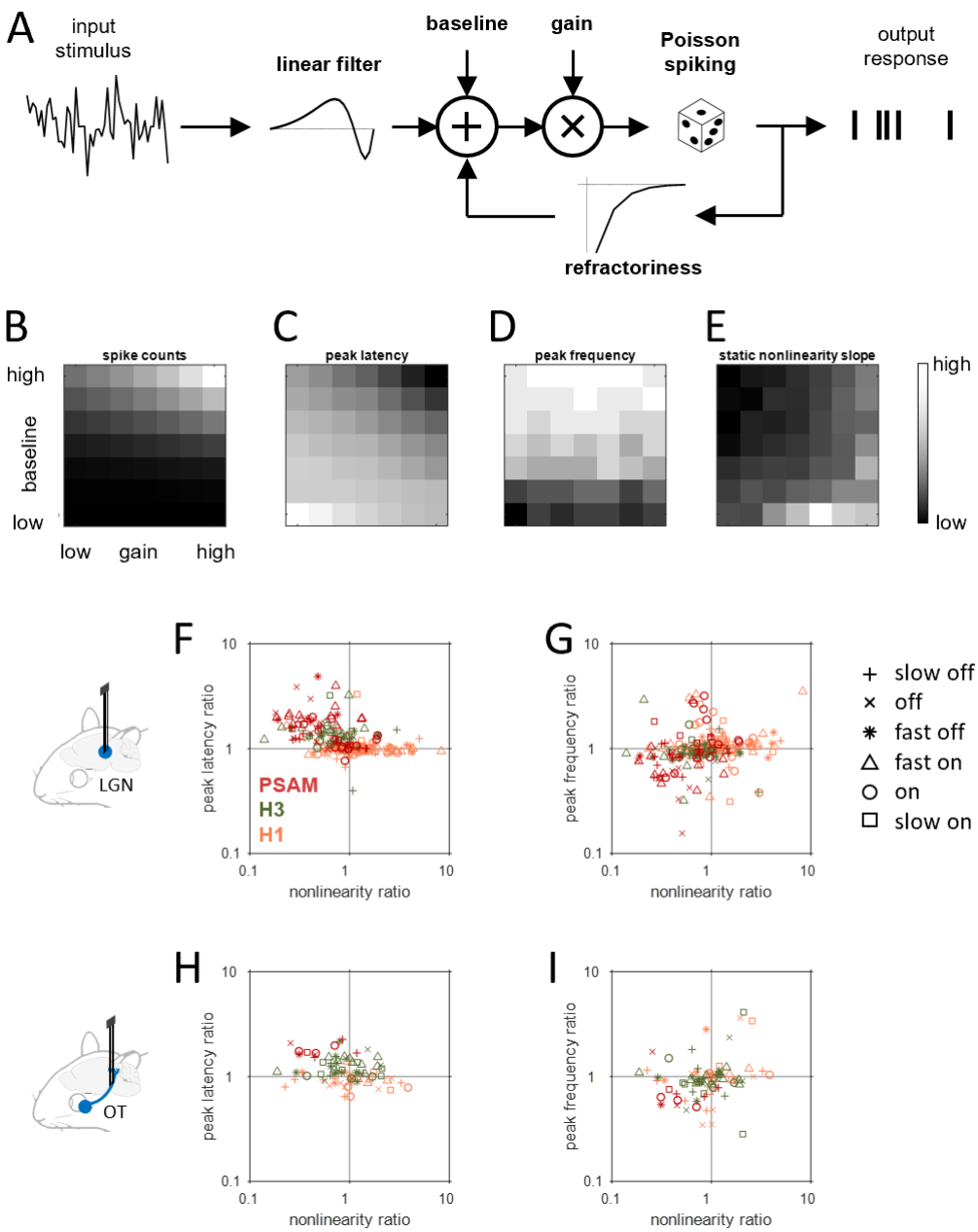

Figure 4: Gain modulation accompanies the peak latency modulation but not the peak frequency modulation via histaminergic effects. *A-E*: Using a computational model outlined in A, here we examined the consequences of varying the baseline and gain levels on the response features, such as spike counts (B), peak latency (C) and frequency (D) of the estimated linear filter from the simulated responses, and slope of static nonlinear gain function of the model neuron (E). See Methods for details. *F,G*: relationship between the magnitudes of the gain modulation and response kinetics modulation by perturbing the histaminergic system for LGN neurons (chemogenetics, red; ciproxifan, green; chlorphenamine, orange; N=222 from 8 animals). A stronger correlation was found for the peak latencies (F, R = –0.42, p<0.001) than for the peak frequencies (G, R = 0.17, p=0.01). *H,I*: corresponding figure panels for RGC responses (N=84 from 9 animals). Significant correlation to the gain modulation was found for the peak latency modulation (R = –0.25, p = 0.02), but not for the peak frequency modulation (R= 0.20, p = 0.07).

Discussion

Here we provide in vivo electrophysiological evidence for histaminergic modulation of the mouse early visual processing: i.e., the more the histamine, the slower and weaker the LGN and RGC responses in awake head-fixed mice (Figures 1 and 2). This is, however, opposite from what one would expect for the effect of histamine, given that the level of brain histamine typically increases as animals become more aroused (Thakker, 2011). At a behavioral level, antihistamine drugs lead to drowsiness in humans, impairing sensory processing (van Ruitenbeek et al., 2009). At neurophysiological level, it has been shown that histamine leads to slow depolarization of LGN relay cells in cats and guinea pigs (McCormick and Williamson, 1991; Uhlrich et al., 2002). Histamine was thus expected to facilitate visual processing, unlike our observations. Discrepancies here may arise from two reasons. Firstly, the effects of histamine can be species-specific. In particular, as nocturnal animals, mice are less active during daytime. Thus, facilitating visual responses at low histamine level may be ethologically beneficial for mice to respond faster to visual threats during daytime, especially when mice are dormant. Future studies in the context of sleep-wake cycles as well as in diurnal animals will give further insights into this question.

Secondly, our unexpected results may be due to differences in experimental conditions. Electrophysiological studies on neuromodulation were conventionally conducted in vitro or in anesthetized animals (McCormick and Williamson, 1991; Uhlrich et al., 2002; Warwick et al., 2024). It has been shown, though, that substantial differences exist in the early visual processing between awake and anesthetized conditions (Durand et al., 2016), including the retinal output (Boissonnet et al., 2023). Here we took a computational modelling approach to better understand the net effect of histamine from functional viewpoints, rather than pursuing the underlying biophysical mechanisms. For example, we suggest that the H1 receptors mediate gain modulation in RGCs: chlorphenamine (H1 antagonist) affected the response latency but not the frequency tuning (Figure 2), a distinctive feature of gain modulation identified by our computational modelling analysis (Figure 4). This action of histamine does

not have to be directly on RGCs expressing the H1 receptors, but can be mediated indirectly by circuit mechanisms. Indeed, histamine affects both inward and outward currents of amacrine cells in the mouse retina (Horio et al., 2018). The effects of histamine can then be more profound than gain modulation, much as we observed diverse outcomes in RGCs and LGN when different pharmacological and chemogenetic perturbation tools were employed (see also Warwick et al., 2024). Furthermore, in awake conditions, the histaminergic system acts in concert with other neuromodulator systems (McCormick et al., 2020). For example, serotonergic neurons in the dorsal raphe nucleus have been suggested to project to the retina (Schütte, 1995; Repérant et al., 2000; Gastinger et al., 2006). As the brain state is dynamically controlled by multiple neuromodulators, it will be critical to further characterize neuromodulation of the retina and downstream visual areas in various behavioral contexts.

What is the biological relevance of such histaminergic modulation of the early visual system, starting from the retina? Growing evidence supports significant correlations between awake retinal responses and various behavioral measures, such as pupil dynamics and locomotion (Schröder et al., 2020; Liang et al., 2020; Boissonnet et al., 2023). We, however, show that resulting changes in pupil size and locomotion behavior by manipulating the histaminergic system were not always consistent with the effects on LGN or RGC visual responses (Figure 3). Therefore, the observed changes in their visual responses were unlikely to be associated with behavioral modulation by histamine. This in turn suggests that histamine may not fully explain fast modulation of RGCs by arousal or locomotion. Additional mechanisms of retinal modulation should then exist, such as the centrifugal serotonergic system (Schütte, 1995; Repérant et al., 2000; Gastinger et al., 2006). Further studies on the function of the retina as a part of the whole organism, but not in isolation, will be critical to better understand sensory information processing in awake animals under natural conditions.

Materials and Methods

No statistical method was used to predetermine the sample size. The significance level was 0.05 (with multiple comparison correction where appropriate) in all analyses unless noted otherwise. All experiments were performed under the license 233/2017-PR and 220/2024-PR from the Italian Ministry of Health, following protocols approved by the Institutional Animal Care and Use Committee at European Molecular Biology Laboratory. The data analyses were done in Python and Matlab.

Animals

Animals were housed on a 12h light-dark cycle, with ad libitum access to water and food. All experiments were performed on female mice. A total of 20 wild-type (C57BL6/J; RRID:IMSR_JAX:000664) and 10 hemizygous HDC-cre (Hdctm1.1(icre)Wwis/J; RRID:IMSR_JAX:021198) mice were used for pharmacological and chemogenetic manipulations, respectively.

Surgical procedures

All surgical procedures were performed in animals from 4 to 19 weeks old (9.2 weeks median age). Before the surgery, animals were injected with Caprofen (5 mg/Kg) and then anaesthetized with isoflurane (4% for induction, 1% for maintenance in O_2). Throughout the surgery, the temperature of the animals was kept stable at 37°C using a heating pad (Supertech Physiological). Ointment (VitA-Pos, Ursapharm) was applied on both eyes to prevent them from drying during the surgery, and the animals were placed in a stereotaxic frame (Stoelting 51625). A portion of the scalp was removed to expose the skull and the periosteum was scraped away with a round scalpel to increase adherence of the dental cement. For those mice belonging to the chemogenetic manipulation group, the skull was aligned in order to level bregma and lambda on the same horizontal plane, and a 100 µm craniotomy was performed using a motorized drill attached to the stereotaxic arm. Viral

392 solution (250 nL; AAV9::FLEX-PSAM Y115F,L141F:5HT3 HC; Vector Biosystems, VB773)
393 was injected with an automatic injector pump at 1nL/sec, at the coordinate of AP: -2.6, ML:
394 ±0.8, DV:-5.3. All animals were then implanted with a custom-made titanium head plate,
395 cemented on the skull using a mixture of cyanoacrylate (Loctite 401, Henkel) and dental
396 cement (Paladur, Kulzer). The head plate featured a hole (8 mm diameter), allowing for clear
397 observation of both bregma and lambda. The skull surface was then glazed with a thick layer
398 of cyanoacrylate in order to support the skull with mechanical, atmospheric and biological
399 protection, while still allowing for visual identification of reference points. After the surgery
400 animals were allowed to recover on a heating pad and then housed in individual cages. During
401 the following seven days, the mice were administered with painkillers (Caprofen) diluted in the
402 drinking water at a concentration of 50 mg/mL.

403 In vivo electrophysiology

404 After recovery from the surgery, animals were habituated to head fixation by placing them in
405 the experimental apparatus over the course of one week, twice a day for up to two hours. On
406 the day of the recording, we first placed the subject animal in the recording set up with its head
407 fixed, and determined the electrode penetration path the target area using the robotic
408 stereotaxic system (StereoDrive, NeuroStar). The animal was then briefly anesthetized (for
409 about 5 minutes) and a hole was drilled around the electrode entry point on the skull. After the
410 removal of the anesthesia, an acute silicone probe (Buzsaki32L, Neuronexus; or P2,
411 Cambridge Neurotech) coated with a fluorescent dye (DiI stain, Invitrogen, D282) was lowered
412 at 5 μm/s using the robotic arm until visual responses were found in the target area.

413 After presenting a battery of visual stimuli, we briefly anesthetized the animal and
414 injected 0.9% saline solution alone or that containing chlorphenamine (H1 antagonist, 5
415 mg/kg), ciproxifan (H3 antagonist, 12 mg/kg), or PSEM (5 mg/kg). About 20 minutes after the
416 injection and removal of the anesthesia, we presented the same battery of visual stimuli to the
417 animal for the second recording session.

418 After all the recording sessions, the electrode position was verified histologically. After
419 retracting the silicon probe, the mice were anesthetized (2.5% Avertin, 16 μL/g, intraperitoneal
420 injection) and perfused with paraformaldehyde (PFA; 4% in phosphate buffer solution). The
421 brain tissue was harvested and post-fixed overnight in 4% PFA at 4°C. Coronal sections of
422 the brain tissue (thickness, 150 μm) were then examined under a fluorescence microscope
423 (Leica, LMD7000 with N2.1 filter cube) to visualize the trace left by the DiI stain on the probe.

424 Visual stimulation

425 Visual stimuli were presented as described before (Boissonnet et al., 2023). Briefly, visual
426 stimuli were projected onto a spherical screen (20cm in radius) painted with ultra-violet (UV)
427 reflective white paint, placed 20 cm from the mouse's left eye. A gamma-corrected digital light
428 processing device (DLP, Texas Instruments, DLPDLCR3010EVM-LC) was used as a light
429 source after the green and the red LEDs were replaced with UV (365nm, LZ1-00UV00, LED
430 Engine) and infrared (IR: 950nm, SFH 4725S, Osram) LEDs respectively. The IR light was
431 used as a synchronization signal and was recorded with a photodiode (PDA100A2, Thorlabs).
432 Stimulation was conducted at 60 frames per second (FPS), and covered 73° in azimuth and
433 44° in altitude from the mouse eye position. The maximum light intensity at the eye position
434 was 31 mW/m^2 (15.4 mW/m^2 for UV LED and 15.9 mW/m^2 for blue LED; measured with S121C
435 sensor, Thorlabs), leading to mesopic to photopic conditions. Using QDSpy software (Franke
436 et al., 2019), we presented the following stimuli: a randomly flickering full-field stimulus (5
437 minutes) consisting of a random sequence of black and white frames at 60 FPS; and a black-
438 and-white binary dense noise stimulus (15 minutes), consisting of a 32-by-18 pixels
439 checkerboard, where each pixel followed an independent random sequence at 60 FPS but the
440 overall luminance of the frame was kept constant at the mean value.

441 Electrophysiology data analysis

442 Raw data from the same animal before and after treatment were concatenated and processed
443 as a single recording. Spike sorting was performed with Kilosort2 for semi-automatic cluster

detection and Phy for visualization and data curation. In total, we recorded 311 RGCs from 18 animals and 421 cells in LGN from 12 mice.

For systematically characterizing the visual response properties, we used stimulus ensemble statistical techniques ("reverse correlation" methods; 500 ms window; $\Delta t = 1/60$ s bin size) to calculate the linear filter and static nonlinear gain function of the recorded cells in response to white-noise stimuli as described before (Figure 1A; Boissonnet et al., 2023). Briefly, we first obtained the linear filter of each cell by calculating a spike-triggered average (STA) of the stimulus with ±1 being "white" and "black," respectively. As a quality measure, p-value was computed for each time bin against a null hypothesis that the STA follows a normal distribution with a mean of zero and a variance of 1/C, where C is the total number of spikes. As a measure of the cell's response kinetics, we then estimated the peak latency by fitting a difference-of-Gaussian curve to the linear filter; and the spectral peak frequency by the Fourier analysis on the linear filter. Spatial response properties were examined for STAs from "checkerboard" stimulation. In particular, we fitted a two-dimensional Gaussian envelope to the spatial filter at the peak latency (e.g., Supplementary Figure 3B,H), and the receptive field (RF) size was estimated as twice the mean standard deviation (SD) of the long and short axes.

The linear temporal filters from full-field white-noise stimuli were used for broadly classifying the response types of RGCs and LGN cells, respectively (Supplementary Figure 1). Specifically, we first used t-Distributed Stochastic Neighbor Embedding (t-SNE) to map the STAs onto two-dimensional space, and then used K-means++ algorithm for heuristically categorizing the responses into the following six types: fast ON, ON, slow ON, fast OFF, OFF, and slow OFF.

Static nonlinear gain function of each cell (bin size, 0.1) was computed as: P(response | stimulus) = N(stimulus | response) / N(stimulus) / Δt, where N(stimulus | response) and N(stimulus) are the distributions of spike-triggered stimulus ensembles projected onto the L2-normalized STA and the entire stimulus ensembles, respectively. The ratio of P(response |

470 stimulus) before and after the treatment was used as a measure of response gain modulation
471 for each cell.

472 Behavioral data analysis

473 For all experiments, the mouse's left eye – i.e., the side presented with visual stimuli – was
474 recorded using an IR camera (The Imaging Source, DMK23UV024) to monitor its motion and
475 pupil dynamics at 30-60Hz. Pupil detection was done using a Mask-Region based
476 Convolutional Neural Network (Mask-RCNN), trained as described previously (Boissonnet et
477 al., 2023). Two-dimensional ellipse was fit to the pupil, and the large axis diameter was used
478 as a measure of the pupil size. We then calculated the mean pupil size during the recording
479 sessions, and used the ratio before and after pharmacologic or chemogenetic treatment as a
480 measure of the treatment effects on the pupil dynamics (Figure 3A).

481 We also monitored the running speed of an animal based on the turning speed of the
482 custom-made rotary treadmill throughout the recordings. We set a threshold at 2 cm/s to detect
483 running behavior. The animals, however, did not run frequently on the treadmill (17 ± 25%,
484 mean ± standard deviation; 30 animals). As a measure of the treatment effects, we thus used
485 a) the ratio of the fraction of the "non-running" period (Figure 3B); and b) that of the average
486 running speed during the recording session before and after pharmacological or chemogenetic
487 treatment (Figure 3C).

488 Model analysis

489 To explore how different aspects of neuronal intrinsic properties and output responses are
490 interrelated between each other, we simulated a model neuron's responses to white-noise
491 stimuli using different model parameter values (Figure 4A), and characterized these simulated
492 responses using a linear-nonlinear cascade model as we did for the experimental data.

493 Specifically, we employed an integrate-and-fire neuron model with Poisson spiking and
494 refractoriness. A model neuron's discrete linear filter (of length n_T = 25) was given by a sine

function with logarithmic scale in time: i.e., $L(i) = \sin[2*\pi*((10^{t_i}-1)/(10^{s_t}-1))]$, where $s_t = 1.5$ is a temporal spacing parameter and $t_i = i*s_t/(n_T-1)$ for $i=0,\ldots,n_T-1$. The spike-generating function V(i) was then modelled by first projecting the white-noise Gaussian stimulus S(i) (of length 1,000,000; normalized to have a maximum value of 1) onto L(i), followed by the addition of baseline B and the multiplication by gain G: i.e., $V(i) = G*(\Sigma_j L(j)*S(i-j) + B)$. For each simulation, we chose the value of B from -0.45 to 0.45 in steps of 0.15; and that of G from 1.2^g with g = -3, -2, -1, 0, 1, 2, 3. The spiking response was then generated by thresholding V(i) (at a random threshold for every time point derived from a uniform distribution from 0 to 1) and refractoriness (given by an exponential filter: $-\exp[-i/s_h]$ for $i = 0,\ldots,5$ with $s_h = 1$). The output spike trains were then subject to the reverse-correlation analysis as described above to characterize the apparent linear filter and static nonlinearity of the model neuron, much as we did for the experimentally recorded RGCs and LGN cells. Specifically, we focused on the peak latency and frequency of the estimated linear filters and the slope of the estimated static nonlinear gain function, and examine how these features depend on the baseline B and the intrinsic gain G of the model neuron (Figure 4B-E).

Acknowledgments

This work was supported by research grants from EMBL (H.A.). The EMBL Advanced Light Microscopy Facility are acknowledged for support in histological image acquisition and analyses, and EMBL IT Support for provision of computer and data storage servers. We thank Dmitry Molotkov, Tom Boissonnet, Vanesa Pelcastre, Sahana Rao, Shabnam Chandel for their help in experiments, and all the Asari lab members for many useful discussions..

References

Bloomfield, S.A., Völgyi, B. (2009). The diverse functional roles and regulation of neuronal gap junctions in the retina. Nat Rev Neurosci. 10(7), 495–506.

Boissonnet, T., Tripodi, M., Asari, H. (2023). Awake responses suggest inefficient dense coding in the mouse retina. Elife. 12, e78005.

Brown, R.E., Sergeeva, O.A., Eriksson, K.S., Haas, H.L. (2002). Convergent Excitation of Dorsal Raphe Serotonin Neurons by Multiple Arousal Systems (Orexin/Hypocretin, Histamine and Noradrenaline). J. Neurosci. 22, 8850–8859.

Chichilnisky, E. J. (2001). A simple white noise analysis of neuronal light responses. Network, 12(2), 199–213.

Durand, S., Iyer, R., Mizuseki, K., de Vries, S., Mihalas, S., Reid, R. C. (2016). A Comparison of Visual Response Properties in the Lateral Geniculate Nucleus and Primary Visual Cortex of Awake and Anesthetized Mice. J Neurosci, 36(48), 12133–12156.

Esposti, F., Johnston, J., Rosa, J. M., Leung, K.-M., Lagnado, L. (2013). Olfactory Stimulation Selectively Modulates the OFF Pathway in the Retina of Zebrafish. Neuron, 79(1), 97-110.

Franke, K., Chagas, A. M., Zhao, Z., Zimmermann, M. J., Bartel, P., Qiu, Y., Szatko, K. P., Baden, T., Euler, T. (2019). An arbitrary-spectrum spatial visual stimulator for vision research. Elife, 8, e48779.

Gastinger, M.J., O'Brien, J.J., Larsen, J.N.B., Marshak, D.W. (1999). Histamine Immunoreactive Axons in the Macaque Retina. Invest. Ophthalmol. Vis. Sci. 40, 487–495.

Greferath, U., Kambourakis, M., Barth, C., Fletcher, E.L., Murphy, M. (2009). Characterization of histamine projections and their potential cellular targets in the mouse retina. Neuroscience 158, 932–944.

Gastinger, M. J., Tian, N., Horvath, T., Marshak, D. W. (2006). Retinopetal axons in mammals: Emphasis on histamine and serotonin. Curr. Eye Res. 31, 655–667.

Haas, H., Panula, P. (2003). The role of histamine and the tuberomamillary nucleus in the nervous system. Nat. Rev. Neurosci. 4, 121–130.

544 Horio, K., Ohkuma, M., Miyachi, E.-I. (2018). The effect of histamine on inward and
545 outward currents in mouse retinal amacrine cells. Cell. Mol. Neurobiol. 38, 757–767.

546 John, J., Wu, M.-F., Boehmer, L.N., Siegel, J.M. (2004). Cataplexy-Active Neurons in the
547 Hypothalamus: Implications for the Role of Histamine in Sleep and Waking Behavior.
548 Neuron 42, 619–634.

549 Kamei, C., Okumura, Y., Tasaka, K. (1993). Influence of histamine depletion on learning
550 and memory recollection in rats. Psychopharmacology (Berl.) 111, 376–382.

551 Khateb, A., Fort, P., Pegna, A., Jones, B.E., Mühlethaler, M. (1995). Cholinergic nucleus
552 basalis neurons are excited by histamine in vitro. Neuroscience 69, 495–506.

553 Khouma, A., Moeini, M.M., Plamondon, J., Richard, D., Caron, A., Michael, N.J. (2023).
554 Histaminergic regulation of food intake. Front. Endocrinol. 14.

555 Klapdor, K., Hasenöhrl, R.U., Huston, J.P. (1994). Facilitation of learning in adult and aged
556 rats following bilateral lesions of the tuberomammillary nucleus region. Behav. Brain Res.
557 61, 113–116.

558 Labandeira-Garcia, J.L., Guerra-Seijas, M.J., Gonzalez, F., Perez, R., Acuña, C., (1990).
559 Location of neurons projecting to the retina in mammals. Neurosci. Res. 8, 291–302.

560 Lee, S.-H., Dan, Y. (2012). Neuromodulation of Brain States. Neuron 76, 209–222.

561 Liang, L., Fratzl, A., Reggiani, J.D.S., El Mansour, O., Chen, C., Andermann, M.L. (2020).
562 Retinal Inputs to the Thalamus Are Selectively Gated by Arousal. Curr. Biol. CB 30, 3923–
563 3934.e9.

564 Lin, W., Xu, L., Zheng, Y., An, S., Zhao, M., Hu, W., Li, M., Dong, H., Li, A., Li, Y., Gong,
565 H., Pan, G., Wang, Y., Luo, Q., Chen, Z. (2023) Whole-brain mapping of histaminergic
566 projections in mouse brain. Proc. Natl. Acad. Sci. U. S. A. 120, e2216231120.

567 Magnus, C.J., Lee, P.H., Bonaventura, J., Zemla, R., Gomez, J.L., Ramirez, M.H., Hu, X.,
568 Galvan, A., Basu, J., Michaelides, M., Sternson, S.M. (2019). Ultrapotent chemogenetics
569 for research and potential clinical applications. Science. 364(6436), eaav5282

570 McCormick, D.A., Nestvogel, D.B., He, B.J., (2020). Neuromodulation of brain state and
571 behaviour. Ann. Rev. Neurosci. 43(1), 391–415.

572 McCormick, D.A., Williamson, A. (1991). Modulation of neuronal firing mode in cat and
573 guinea pig LGNd by histamine: possible cellular mechanisms of histaminergic control of
574 arousal. J. Neurosci. 11 (10), 3188–3199.

575 Mochizuki, T., Yamatodani, A., Okakura, K., Horii, A., Inagaki, N., Wada, H. (1992).
576 Circadian rhythm of histamine release from the hypothalamus of freely moving rats.
577 Physiol. Behav. 51, 391–394.

578 Orsetti, M., Ghi, P., Carlo, G.D. (2001). Histamine H3-receptor antagonism improves
579 memory retention and reverses the cognitive deficit induced by scopolamine in a two-trial
580 place recognition task. Behav. Brain Res. 124, 235–242.

581 Parmentier, R., Ohtsu, H., Djebbara-Hannas, Z., Valatx, J.-L., Watanabe, T., Lin, J.-S.
582 (2002). Anatomical, Physiological, and Pharmacological Characteristics of Histidine
583 Decarboxylase Knock-Out Mice: Evidence for the Role of Brain Histamine in Behavioral
584 and Sleep–Wake Control. J. Neurosci. 22, 7695–7711.

585 Pierce, M.E., Sheshberadaran, H., Zhang, Z., Fox, L.E., Applebury, M.L., Takahashi, J.S.
586 (1993). Circadian regulation of iodopsin gene expression in embryonic photoreceptors in
587 retinal cell culture. Neuron 10, 579–584.

588 Reggiani, J.D.S., Jiang, Q., Barbini, M., Lutas, A., Liang, L., Fernando, J., Deng, F., Wan,
589 J., Li, Y., Chen, C., Andermann, M.L. (2023). Brainstem serotonin neurons selectively gate
590 retinal information flow to thalamus. Neuron 111, 711–726.e11.

Repérant, J., Médina, M., Ward, R., Miceli, D., Kenigfest, N.B., Rio, J.P., Vesselkin, N.P. (2007). The evolution of the centrifugal visual system of vertebrates. A cladistic analysis and new hypotheses. Brain Res. Rev. 53, 161–197.

Repérant, J., Araneda, S., Miceli, D., Medina, M., Rio, J. P. (2000). Serotonergic retinopetal projections from the dorsal raphe nucleus in the mouse demonstrated by combined [3H] 5-HT retrograde tracing and immunolabeling of endogenous 5-HT. Brain Res. 878, 213–217.

Rubio, S., Begega, A., Santin, L.J., Arias, J.L. (2002). Improvement of spatial memory by (R)-α-methylhistamine, a histamine H3-receptor agonist, on the Morris water-maze in rat. Behav. Brain Res. 129, 77–82.

Scammell, T.E., Jackson, A.C., Franks, N.P., Wisden, W., Dauvilliers, Y. (2018). Histamine: neural circuits and new medications. Sleep 42, zsy183.

Schröder, S., Steinmetz, N.A., Krumin, M., Pachitariu, M., Rizzi, M., Lagnado, L., Harris, K.D., Carandini, M. (2020). Arousal Modulates Retinal Output. Neuron 107, 487–495.e9.

Schütte, M. (1995). Centrifugal innervation of the rat retina. Vis. Neurosci. 12, 1083–1092.

Takahashi, K., Lin, J.-S., Sakai, K. (2006). Neuronal activity of histaminergic tuberomammillary neurons during wake-sleep states in the mouse. J. Neurosci. Off. J. Soc. Neurosci. 26, 10292–10298.

Thakkar, M.M. (2011). Histamine in the regulation of wakefulness. Sleep Med Rev. 15(1), 65-74.

Uhlrich, D. J., Manning, K. A., Xue, J.-T.. (2002). Effects of activation of the histaminergic tuberomammillary nucleus on visual responses of neurons in the dorsal lateral geniculate nucleus. J. Neurosci. 22, 1098–1107.

Valdés, J.L., Sánchez, C., Riveros, M.E., Blandina, P., Contreras, M., Farías, P., Torrealba, F. (2010). The histaminergic tuberomammillary nucleus is critical for motivated arousal. Eur. J. Neurosci. 31, 2073–2085.

van Ruitenbeek, P., Vermeeren, A., Smulders, F.T.Y., Sambeth, A., Riedel, W.J. (2009). Histamine H1 receptor blockade predominantly impairs sensory processes in human sensorimotor performance. Br. J. Pharmacol. 157, 76–85.

Wang, Y.-Q., Li, R., Wu, X., Zhu, F., Takata, Y., Zhang, Z., Zhang, M.-Q., Li, S.-Q., Qu, W.-M. (2015). Fasting activated histaminergic neurons and enhanced arousal effect of caffeine in mice. Pharmacol. Biochem. Behav. 133, 164–173.

Warwick, R.A., Riccitelli, S., Heukamp, A.S., Yaakov, H., Swain, B.P., Ankri, L., Mayzel, J., Gilead, N., Parness-Yossifon, R., Di Marco, S., Rivlin-Etzion, M. (2024). Top-down modulation of the retinal code via histaminergic neurons of the hypothalamus. Sci Adv. 10(35):eadk4062.

Wilson, M., Lindstrom, S.H. (2011). What the bird's brain tells the bird's eye: the function of descending input to the avian retina. Vis Neurosci, 28(4), 337–350.